AGU PUBLICATIONS

JGR

Journal of Geophysical Research: Atmospheres

RESEARCH ARTICLE

10.1002/2016JD025231

Monotonic decrease of the zonal SST gradient of the equatorial Pacific as a function of CO_2 concentration in CCSM3 and CCSM4

Jun Yang[1], Wm. Richard Peltier[2], and Yongyun Hu[1]

[1]Laboratory for Climate and Atmosphere-Ocean Studies, Department of Atmospheric and Oceanic Sciences, School of Physics, Peking University, Beijing, China, [2]Department of Physics, University of Toronto, Toronto, Ontario, Canada

Key Points:
- Zonal SST gradient of the equatorial Pacific is an almost monotonically decreasing function of CO_2 concentration in CCSM3 and CCSM4
- Enhanced cloud shortwave cooling in the western and central Pacific promotes the weaker zonal SST gradient
- Ocean adjustment to weakened zonal surface winds is characterized by relaxations of the thermocline tilt, zonal currents, and upwelling

Correspondence to:
Yongyun Hu,
yyhu@pku.edu.cn

Citation:
Yang, J., W. R. Peltier, and Y. Hu (2016), Monotonic decrease of the zonal SST gradient of the equatorial Pacific as a function of CO_2 concentration in CCSM3 and CCSM4, *J. Geophys. Res. Atmos.*, *121*, doi:10.1002/2016JD025231.

Received 16 APR 2016
Accepted 4 AUG 2016
Accepted article online 9 AUG 2016

Abstract The west-east sea surface temperature (SST) gradient in the equatorial Pacific Ocean is a key feature of Earth's climate. How this gradient responds to varying climatic forcing is a challenge to both climate theory and climate modeling. Using the coupled atmosphere-ocean general circulation models, Community Climate System Model version 3 (CCSM3) and version 4 (CCSM4), we show that the zonal SST gradient is an almost monotonically decreasing function of atmospheric CO_2 concentration (pCO_2) across a wide range from 17.5 to 4576 ppmv. As pCO_2 is increased, the optical depth of clouds over the western and central Pacific increases significantly, reflecting more insolation back to space, suppressing surface warming in this region and thereby reducing the zonal SST gradient. Ocean adjustment to a weakening of surface zonal winds is characterized by relaxations of the equatorial thermocline tilt, zonal surface currents, and ocean upwelling.

1. Introduction

The zonal sea surface temperature (SST) gradient across the equatorial Pacific Ocean is an important characteristic of the Earth's climate system. The strength of the zonal SST gradient influences the behavior of the El Niño–Southern Oscillation (ENSO), and surface temperature and precipitation in remote regions through the action of atmospheric teleconnections [*Alexander et al.*, 2002; *Chiang*, 2009]. Much effort has been expended in the exploration of the change of the zonal SST gradient with increased levels of anthropogenic greenhouse gases [*Collins and CMIP Modeling Groups*, 2005, 2010; *Liu et al.*, 2005; *Meehl et al.*, 2007; *Vecchi et al.*, 2008; *Dinezio et al.*, 2009; *Xie et al.*, 2010; *Yeh et al.*, 2012; *An et al.*, 2012; *Song and Zhang*, 2014; *Luo et al.*, 2015; *Li et al.*, 2015]. The trend of this gradient in observations over the instrumental record, however, has remained unclear, perhaps due to the poor spatial and temporal sampling of SSTs [e.g., *Tung and Zhou*, 2010; *Deser et al.*, 2012]. In climate simulations, the sign and magnitude of the trend of the zonal SST gradient also appears to be highly model dependent [e.g., *Collins and CMIP Modeling Groups*, 2005; *Yeh et al.*, 2012]. Some models project a decreasing trend of the zonal SST gradient as the climate warms, with SSTs of the eastern Pacific warming more than those in the western Pacific, but other models suggest that the opposite effect should be obtained. The contradictory nature of these results may be due to the fact that the strengths of contributing feedback mechanisms differ significantly between different climate models and to the fact that the range of pCO_2 variations that have been investigated has been small.

Previous studies have suggested that various processes associated with atmosphere, ocean, and their coupling can influence the response of the zonal SST gradient to external forcing.

1. Evaporative cooling: Due to the facts that the surface evaporative cooling rate increases with increasing temperature and that the western Pacific is warmer than the eastern Pacific, the evaporative cooling has a stronger damping effect in the western Pacific than in the eastern Pacific. The zonal SST gradient therefore decreases as atmospheric pCO_2 is increased [*Hartmann and Michelsen*, 1993; *Knutson and Manabe*, 1995; *Merlis and Schneider*, 2011].
2. Cloud response: As climate warms, the western Pacific may exhibit a negative, stabilizing cloud feedback, which would suppress the warming of the warm pool and thereby reduce the zonal SST gradient [*Meehl and Washington*, 1996; *Dinezio et al.*, 2009; *Li et al.*, 2016].
3. The ocean dynamical thermostat mechanism: When a uniform heating is employed to force the ocean, the ocean dynamical response leads to a weaker warming in the east than in the west, promoting a stronger zonal SST gradient [*Clement et al.*, 1996; *Vecchi et al.*, 2008; *Fang and Wu*, 2008].

4. The Walker circulation: As climate warms, the strength of the Walker circulation decreases. This is due to increased static stability in the tropics [*Knutson and Manabe*, 1995], and the magnitude of the decrease is constrained by the different rates of global precipitation and near-surface specific humidity increases to global warming [*Held and Soden*, 2006; *Vecchi et al.*, 2006]. The weakening of the Walker circulation can produce a relaxed zonal SST gradient through its effect on surface wind stresses and in turn on ocean upwelling in the eastern Pacific; the Bjerknes feedback further amplifies this effect [*Bjerknes*, 1969; *Wyrtki*, 1975].
5. Extratropical effect through the ocean: The temperature of the water upwelled in the cold tongue is connected to the wind-driven shallow subtropical-tropical cells (STCs) that transport water from the subtropics to the subsurface of the equatorial Pacific, so changes of SSTs in the subtropics (for example, through increasing or decreasing the cloud albedo and therefore surface shortwave/longwave fluxes in the subtropics [*Barreiro and Philander*, 2008; *Burls and Fedorov*, 2014a]) can influence the SSTs of the equatorial Pacific [*Liu and Huang*, 1997].
6. Extratropical effect through atmosphere: Atmospheric heat transport from the deep tropics to the subtropical region is critical factor in stabilizing the climate of the entire tropics [*Wallace*, 1992; *Pierrehumbert*, 1995]. The nearly saturated, convective deep tropics are unable to dispose of its excess energy, which must be transported to the dry subtropical region ("radiator fins"), where energy is easily emitted to space through infrared radiation. This process acts to suppress the increase of SSTs in the warm pool region and therefore may weaken the meridional as well as zonal SST gradients.
7. Atmospheric superrotation: In a warmer climate, atmospheric convection may be stronger and the associated Rossby waves may produce a stronger equatorward momentum transport, which acts to weaken the equatorial easterlies. The weaker trade winds will relax the Pacific thermocline and thereby promote a smaller zonal SST gradient [*Tziperman and Farrell*, 2009]. In a coupled atmosphere-ocean climate system, all the seven mechanisms described above may work together to control the zonal SST gradient of the equatorial Pacific.

In the past, the zonal SST gradient is expected to have been different from the present-day condition. Geochemical proxy records suggest that the west-east SST contrast gradually increased from 2–3°C in the early Pliocene 5.3 million years ago (Ma) to the present-day value of 5–6°C by 2–1 Ma [*Wara et al.*, 2005; *Fedorov et al.*, 2006, 2013], although this is still in intense debate [*Zhang et al.*, 2014; *Watanabe et al.*, 2011; *Scroxton et al.*, 2011; *Molnar and Cane*, 2007]. The mechanism for the very weak zonal SST gradient characteristic of the early Pliocene is the subject of ongoing and intense investigations. One of the contending explanations is that associated with ocean mixing [*Fedorov et al.*, 2010]. An increase of ocean mixing in the subtropical Pacific might be expected to reduce the poleward ocean heat transport from the equatorial Pacific to the subtropics, deepening the tropical thermocline and warming the surface of the eastern Pacific. Such an increase of ocean mixing could be driven by more frequent and/or stronger tropical cyclones [*Emanuel*, 2001], although whether this mechanism is sufficient or not is still in debate [*Jansen and Ferrari*, 2009]. Other mechanisms have also been proposed, such as changes of the strength and/or direction of equatorial trade winds [*Tziperman and Farrell*, 2009], or changes of cloud albedo in the extratropics [*Barreiro and Philander*, 2008; *Burls and Fedorov*, 2014a, 2014b]. However, to date, no climate model has been able to successfully reproduce the climate state of the early Pliocene suggested by geochemical proxy records, since the atmospheric pCO_2 in this era is believed to have been only moderately higher than the preindustrial level [*Haywood et al.*, 2013, 2016].

One way to gain insight into the dominant physical mechanism(s) underlying the variations of the zonal SST gradient is to investigate its response to extreme climatic conditions, such that the signal would be expected to overwhelm the weak and contradictory variations associated with the differing strengths of various feedback mechanisms that are characteristic of different climate models. Using two fully coupled atmosphere-ocean models, our purpose is to investigate the response of the zonal SST gradient to a wide range of atmospheric pCO_2 conditions. The pCO_2 in our simulations will be chosen to cover values from $\frac{1}{16}$ to 16 times the preindustrial level of 286 ppmv. In comparison with doubling and quadrupling of pCO_2 experiments that have usually been investigated, these larger perturbations in greenhouse gas forcing are found to be sufficient to allow us to much more clearly identify the trend of the zonal SST gradient and to understand the mechanisms responsible for the trend, as previously suggested by *Cherchi et al.* [2008].

The paper is structured as follows. Section 2 contains brief model descriptions and numerical experimental design. We present the response of the zonal SST gradient to variations of pCO_2 and discuss the mechanisms responsible for the trend in section 3. We find that the main mechanism that contributes to the weakening

trend of the zonal SST gradient as pCO_2 is increased is that associated with the change of cloud radiative effects. Discussions and conclusion are provided in sections 4 and 5, respectively.

2. Methods

We employ two climate models, CCSM3 and CCSM4, both developed at the U.S. National Center for Atmospheric Research. Both are fully coupled atmosphere-ocean-land-sea ice general circulation models linked via a coupler with no flux correction between the four components [*Collins et al.*, 2006a; *Gent et al.*, 2011, and references therein]. Relatively low resolution versions of both models are employed for the climate simulations here, a necessity given the large number of simulations required to cover the extensive parameter space of interest to us. The atmospheric module in both models has an Eulerian spectral dynamical core with a transform grid of T31 resolution, 3.75° by 3.75°. The accompanying ocean model has a 3.6° resolution in the zonal direction but a variable resolution in the meridional direction with a spacing of 0.9° near the equator and of 3° in high latitudes. The ocean model has 25 nonequally spaced vertical levels in CCSM3, but 60 levels in CCSM4. In comparison with CCSM3, CCSM4 has significantly improved representations and parameterizations for atmospheric deep convection, sea ice thermodynamics, land water storage, surface ocean currents, and deep ocean overflows. In particular, CCSM4 is able to well simulate the spatial and temporal patterns of ENSO. The ENSO spectrum of CCSM4 contains significantly more power at low frequency and is much closer to observations, compared to CCSM3 [*Deser et al.*, 2012].

Sixteen experiments with different pCO_2 have been carried out. The pCO_2 values are set to 35, 70, 140, 286, 572, 1144, 2288, and 4576 ppmv in CCSM3, and to 17.5, 35, 70, 140, 286, 572, 1144, and 2288 ppmv in CCSM4. The pCO_2 for each model is the only parameter varied between the simulations. The equatorial Pacific in CCSM4 is generally approximately 2°C warmer than that of CCSM3 for the same level of pCO_2 (Figures 1c and 1d) and closer to observations [see *Gent et al.*, 2011]. For this reason, we use the different pCO_2 sequences for the two models, in order to compensate for the difference in equatorial mean state temperature. Other greenhouse gases in all simulations are fixed at their preindustrial levels, namely, 805.6 ppbv for CH_4, 276.7 ppbv for N_2O, and no CFCs. Solar constant, orbital parameters, land-sea distribution, surface topography, and ocean bathymetry are all maintained at their present-day conditions.

All of the experiments have been initialized from a preindustrial climate state by abruptly decreasing or increasing pCO_2. For the experiments with 286 ppmv of CO_2, the integration of the model has been continued for 700 years in order to reach a new statistical equilibrium; each of the other simulations is integrated for 1200–2000 years. The last 100 year characterization of the new equilibrium is employed as basis for analysis. In calculating the linear trends of variables (such as SST) for each doubling of CO_2 concentration, we first compute the averages of the 100 year data set for each CO_2 experiment and then compute the linear trends among different CO_2 concentration experiments. In the experiments with the highest pCO_2 (such as the 2288 ppmv CO_2 experiment in CCSM4), the deep ocean has yet reached statistical equilibrium during the integration, which nevertheless has only a small effect on the ocean stratification (see Figure 10f and following text). Note that even in the lowest CO_2 cases, the sea ice edge never enters the tropics, so that sea ice cannot be expected to have any direct effect on the equatorial SSTs to be discussed in what follows. In order to obtain a globally ice-covered snowball state, a further decrease of the solar constant by 5–6%, in addition to the marked reduction in pCO_2 would be required [*Yang et al.*, 2012a, 2012b].

3. Results

3.1. Sea Surface Temperature Response

As atmospheric pCO_2 is gradually increased from a very low level (35 ppmv in CCSM3 or 17.5 ppmv in CCSM4) to a very high level (4576 ppmv in CCSM3 or 2288 ppmv in CCSM4), surface temperatures increase due to the increasing strength of the greenhouse effect (Figures 1a and 1b), but the changes of SST along the equatorial Pacific are variable as a function of longitude (Figures 1c and 1d). In CCSM3, the warming in the central and eastern Pacific is greater than that in the western Pacific, and the zonal SST gradient decreases but only to the west of the date line (Figure 2a). This linear pattern of CCSM3 is similar to that of the multimodel mean response to CO_2 doubling in the World Climate Research Program Coupled Model Intercomparison Project phase-3 data set (CMIP3) [*Dinezio et al.*, 2009]. In CCSM4, the zonal SST gradient exhibits a significantly decreasing trend across the entire deep tropical Pacific Ocean, with the maximum warming occurring around the center of the cold tongue (Figure 2b). When the west-east SST contrast is defined by the SST

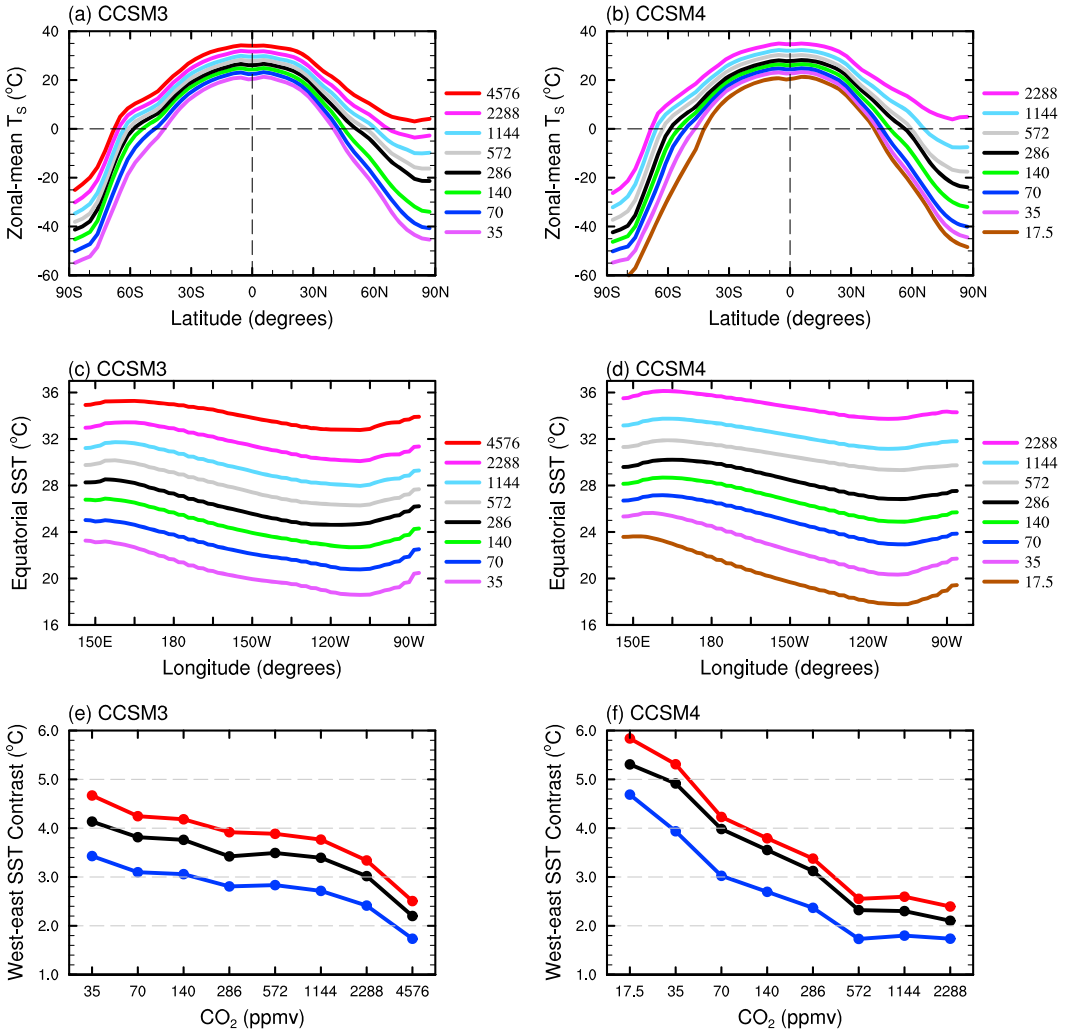

Figure 1. (a, b) Annual- and zonal-mean surface air temperature (T_S); (c, d) annual-mean sea surface temperature (SST) along the equatorial Pacific (5°S–5°N); (e, f) west-east SST contrast. The west-east SST contrast is defined by the maximum minus the minimum (red dots), the difference between [5°S to 5°N, 150°E to 170°E] and [5°S to 5°N, 115°W to 95°W] (black dots), or the difference between [10°S to 10°N, 150°E to 170°E] and [10°S to 10°N, 115°W to 95°W] (blue dots). Left column is for CCSM3 and right column for CCSM4. The CO_2 concentrations in CCSM3 are from 35 to 4576 ppmv and in CCSM4 from 17.5 to 2288 ppmv.

average of the western Pacific (5°S–5°N, 145°E–165°E) minus the SST average of the eastern Pacific (5°S–5°N, 120°W–100°W), it is found that the west-east SST contrast is a nearly monotonically decreasing function of pCO_2 in both CCSM3 and CCSM4 (Figures 1e and 1f). For each doubling of pCO_2, the decrease of the contrast is between 0.1 and 1.0°C. The use of slightly different definitions leads to a rather similar decreasing trend of the gradient although the magnitudes differ somewhat (Figures 1e and 1f).

3.2. Cloud Responses

Cloud responses act to decrease the zonal SST gradient in both CCSM3 and CCSM4, as shown in Figure 3. On the basis of the experiments covering a wide range of pCO_2, it is clear that the cloud feedback has a cooling effect on the surface over the western Pacific but a warming effect over the eastern Pacific (Figures 3m and 3n). This west-east asymmetric change in clouds promotes a weaker zonal SST gradient as pCO_2 is increased. The different cloud feedbacks over the western and eastern Pacific is due to the fact that the former is in a deep convection regime while the latter is in large-scale subsidence regime [*Meehl and Washington*, 1996]. For each doubling of pCO_2, the change of net (shortwave plus longwave) cloud radiative effect is on the order of

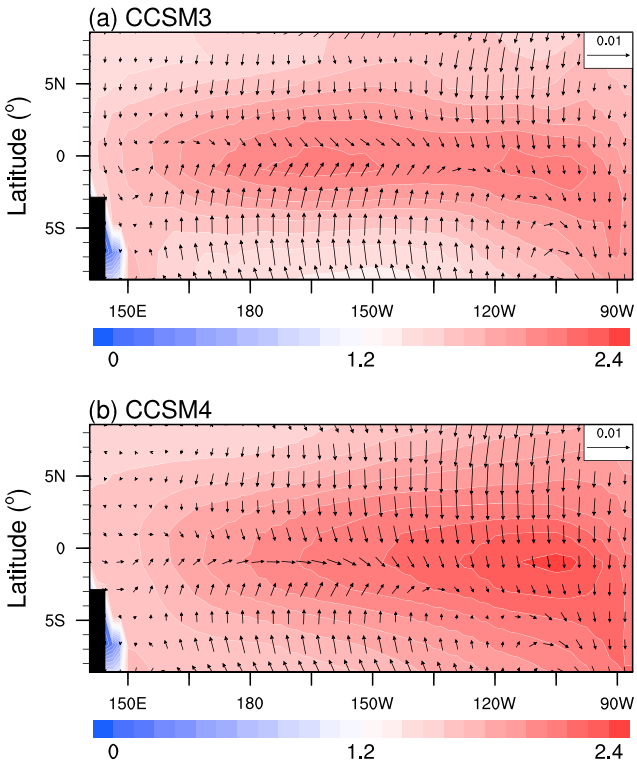

Figure 2. Linear trends of deep tropical sea surface temperatures (K, shading) and surface wind stresses (0.01 N m^{-2}, vectors) for each doubling of CO_2 concentration in (a) CCSM3 and (b) CCSM4.

1 to 10 W m^{-2}, which is comparable to the change of CO_2 greenhouse effect (≈3.7 W m^{-2} at the tropopause [*Boucher et al.*, 2001]; note that there is a significant uncertainty in this number [see *Collins et al.*, 2006b, Figure 4]).

As the climate warms, atmospheric water vapor content increases, generally following the Clausius-Clapeyron relation. The significant increase of water vapor content results in the supply of more moisture for the formation of clouds especially in the deep convection region of the western Pacific (Figures 3g and 3h). Meanwhile, cloud coverage increases especially for high- and middle-level clouds above the level of 700 hPa (Figures 3c and 3f). Both effects increase the optical depth of the clouds over the western Pacific, reflecting more solar radiation back to the space and suppressing the warming of the surface in this region. The cloud longwave radiative effect also increases (Figures 3k and 3l), mainly due to the increase of high-level cloud coverage above the level of 400 hPa (Figures 3e and 3f). The high-level clouds absorb longwave radiation from the warmer (relative to cloud temperature) surface but emit longwave energy to the space and to the surface at the cloud temperature, so that they have a warming effect on the surface. The low-level cloud coverage below the level of 700 hPa exhibits a small increasing trend in the western and central Pacific and a small decreasing trend in the eastern Pacific (Figures 3a and 3b), so the low-level cloud coverage trend also has a net effect of decreasing the zonal SST gradient, but its magnitude is much smaller than the changes of cloud water content and high- and middle-level cloud coverage.

Besides the changes of clouds in the deep tropics, clouds in the subtropics also change. In general, the cloud albedo decreases in the subtropics around 30°S(N), and the net (shortwave plus longwave) cloud effect is positive there (figure not shown), which has a warming effect on the atmosphere and the surface and thereby decreases the meridional SST gradient. Through the wind-driven oceanic subtropical-tropical cells (STCs), this cloud response would have a potential effect of increasing the SSTs in the cold tongue region and thereby would decrease the zonal SST gradient along the equator, as the mechanism first proposed by *Barreiro and Philander* [2008].

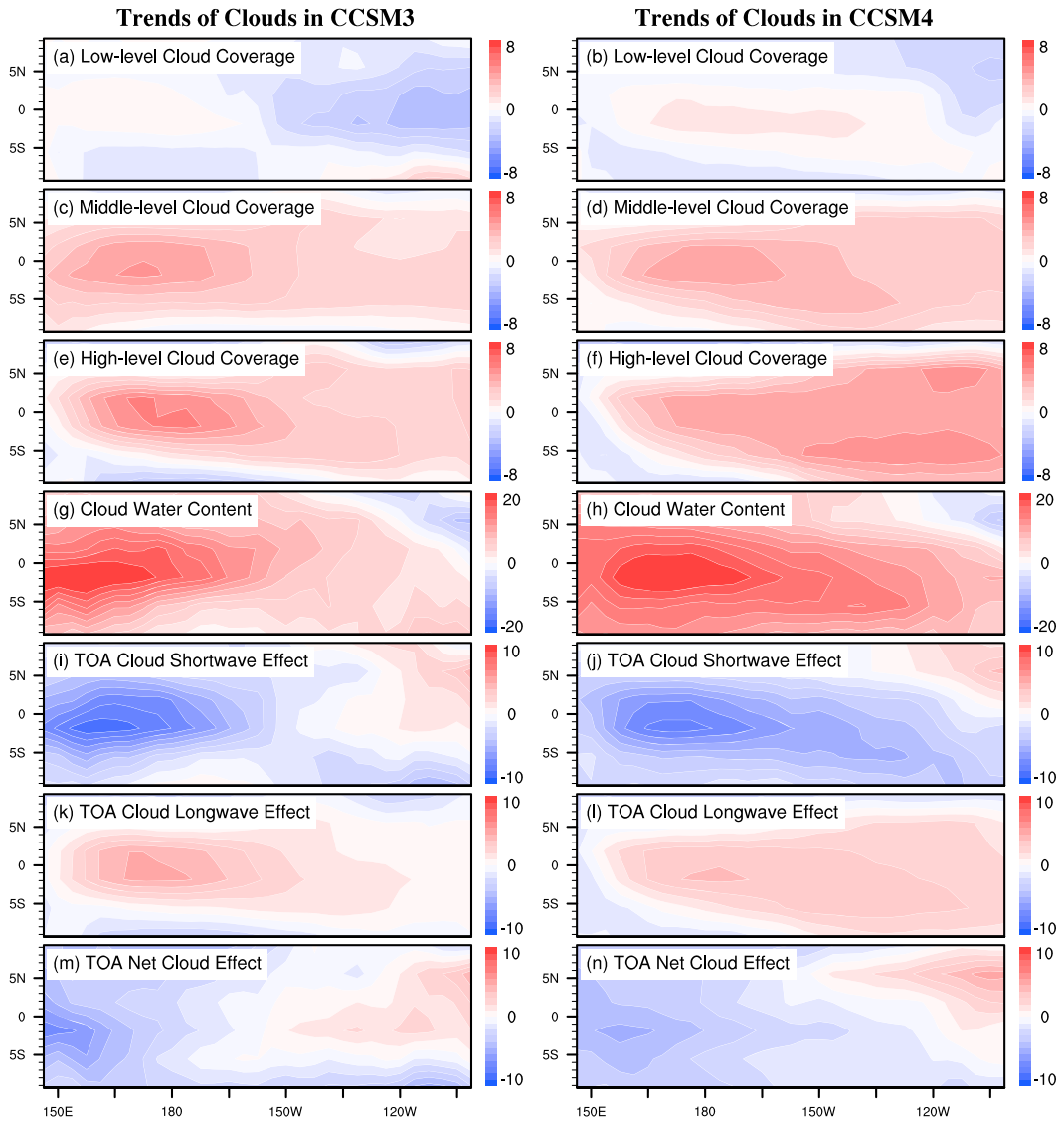

Figure 3. Linear trends of clouds for each doubling of CO_2 concentration. Linear trends of (a, b) low-level (below 700 hPa) cloud coverage, (c, d) middle-level (between 700 and 400 hPa) cloud coverage, (e, f) high-level (above 400 hPa) cloud coverage, (g, h) vertically integrated cloud water (liquid plus ice) content, (i, j) cloud shortwave radiative effect at the top of the atmosphere (TOA), (k, l) TOA cloud longwave radiative effect, and (m, n) TOA cloud net radiative effect. The unit of cloud coverage is percent, cloud water content g m^{-2}, and cloud radiative effect W m^{-2}. Left column is for CCSM3 and right column for CCSM4.

3.3. Changes in Surface Energy Fluxes

In equilibrium, surface temperature is determined by surface energy balance, and the surface energy budget can be expressed as

$$SW + LW + LH + SH = Q_{net} \quad (1)$$

where SW is all-sky net shortwave flux (downward plus upward), LW is all-sky net longwave flux, LH is surface latent heat flux, SH is surface sensible heat flux, and Q_{net} is heat flux into the ocean, which should be balanced by the divergence of ocean heat transport through horizontal and vertical advection and diffusion. Since the diffusion terms are not stored as a part of model output at run time, we can only infer the values of Q_{net} as a residual term in the balance term of equation (1). All the fluxes and their trends are defined as downward positive and upward negative.

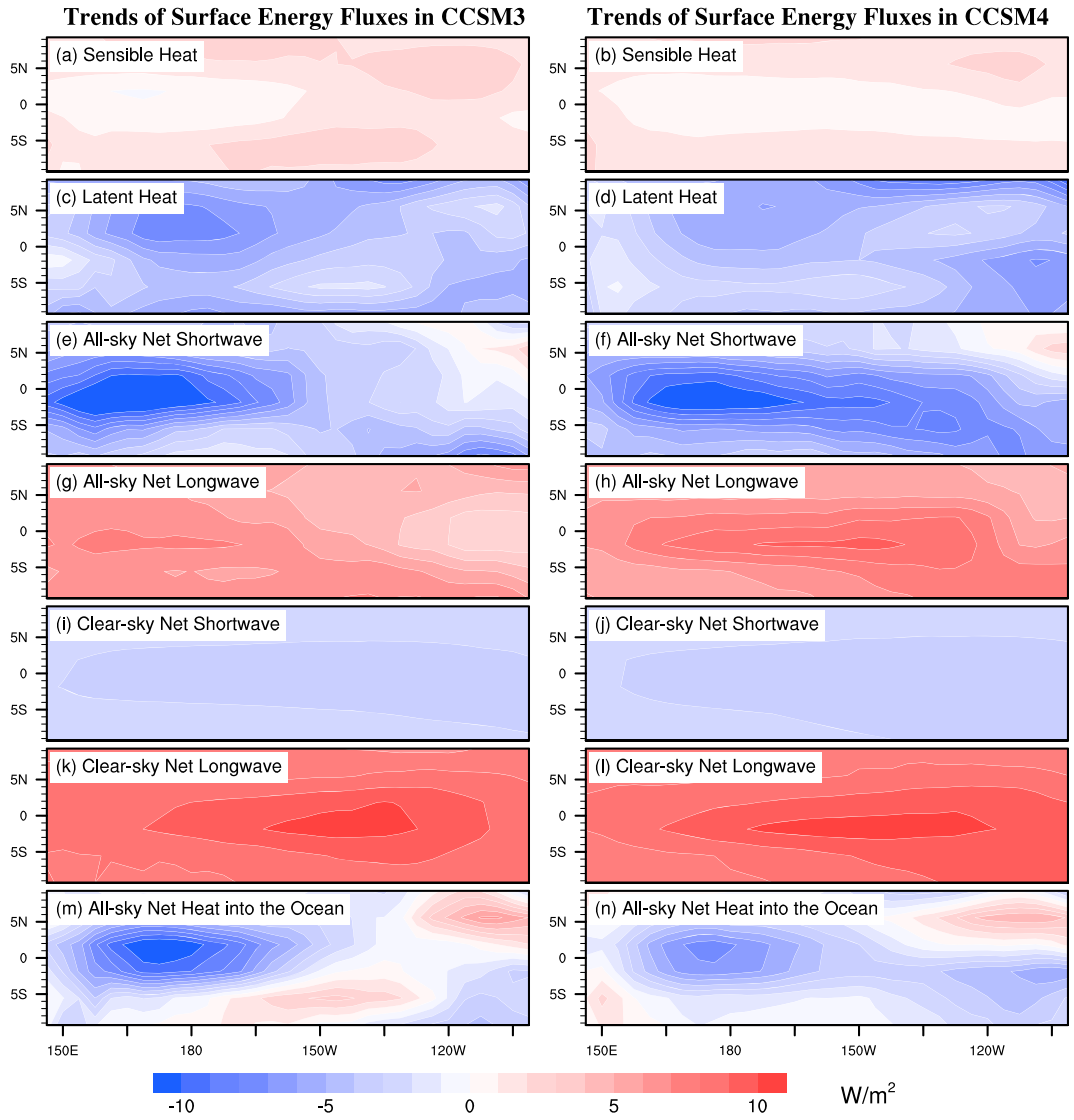

Figure 4. Linear trends of surface (a, b) sensible heat flux, (c, d) latent heat flux, (e, f) all-sky net (downward minus upward) shortwave flux, (g, h) all-sky net longwave flux, (i, j) clear-sky net shortwave flux, (k, l) clear-sky net longwave flux, and (m, n) all-sky net heat flux into the ocean, for each doubling of CO_2 concentration. The contour interval is 1 W m^{-2} in all the panels. Left column is for CCSM3 and right for CCSM4. Positive values imply heating of the ocean surface.

Figure 4 shows the trends of surface energy fluxes, including all-sky SW, all-sky LW, LH, SH, clear-sky SW, clear-sky LW, and all-sky Q_{net}, for each doubling of pCO_2. It is found that

1. the trend of SH is much smaller than other energy fluxes (Figures 4a and 4b), so it has a negligible effect on the surface temperature and on the zonal SST gradient;
2. the trend of LH is significant, but there is no significant asymmetry between the western equatorial Pacific and the eastern equatorial Pacific (Figures 4c and 4d), so that the evaporative cooling mechanism proposed by *Hartmann and Michelsen* [1993] and *Knutson and Manabe* [1995] is not very significant in our simulations;
3. the trend of all-sky SW is the most pronounced, and the magnitude of the decrease in the western Pacific is much larger than that in the eastern Pacific (Figures 4e and 4f); the main contribution is from the change of the cloud shortwave radiation effect (see Figures 3i and 3j);
4. the trend of all-sky LW shows an asymmetry between the west and the east in CCSM3 (Figure 4g), but its magnitude is much smaller than that of all-sky SW. In CCSM4, the trend of all-sky LW shows an equatorially enhanced pattern and no significant asymmetry between the west and the east (Figure 4h).

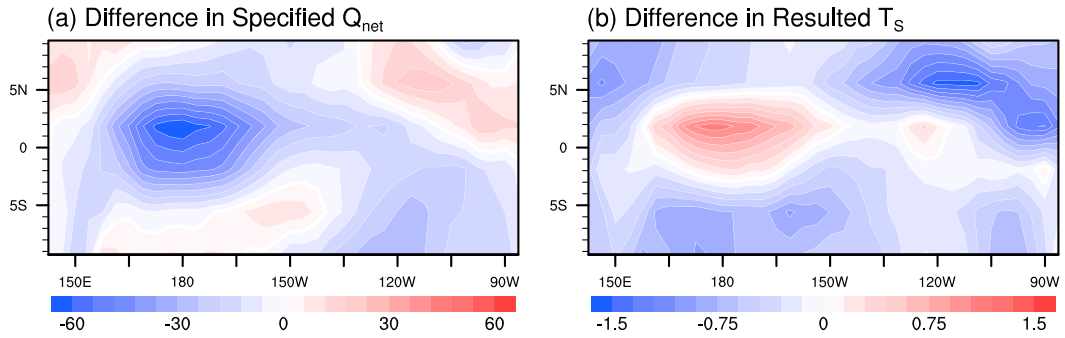

Figure 5. (a) Difference in the specified surface heat flux into the ocean (Q_{net}, W m^{-2}) and (b) difference in the resulted surface temperature (T_S, K), simulated by the atmospheric component of CCSM3, which is CAM3, coupled to a 50 m slab ocean. The CO_2 concentration is 4576 ppmv in both experiments.

In clear-sky radiative transfer calculations (i.e., the calculations of radiative fluxes using the same surface temperature, temperature profile, CO_2 concentration, water vapor content, but without cloud radiative effects), SW also decreases, but with a much smaller magnitude than that of all-sky SW, and it has a nearly uniform spatial pattern (Figures 4i and 4j). The change of clear-sky SW is due to the fact that water vapor concentration in the air increases as the climate warms, which leads to the absorption of more shortwave radiation and allows less shortwave radiation to reach the surface. The clear-sky LW shows a zonally asymmetry pattern, in which the central Pacific has a stronger trend than the western Pacific (Figures 4k and 4l), which implies that the increase of clear-sky greenhouse effect due to the increase of water vapor concentration and to the adjustment of temperature profile is larger in the central Pacific than in the western Pacific. This promotes a decrease of the zonal SST gradient to the west of 180°W, but its magnitude is only about 25% of the change of all-sky SW.

Figures 4m and 4n show the trend of all-sky Q_{net} for each doubling of pCO_2. It is found that Q_{net} decreases in the western and central Pacific, increases in the northeast Pacific, and decreases in the southeast Pacific; the maximum decrease of Q_{net} is in the warm pool region rather than in the cold tongue region in both models. In order to know how the change of Q_{net} affects the zonal SST gradient, two further experiments are run. We employ the atmospheric component of CCSM3, which is CAM3, coupled to a uniform 50 m slab ocean. In the two experiments, the model setup is the same (such as a 4576 ppmv CO_2) except that one is with the Q_{net} of the CCSM3 experiment with 286 ppmv CO_2, and the other one is with the Q_{net} of the CCSM3 experiment with 4576 ppmv CO_2. The difference in deep tropical surface temperatures is shown in Figure 5b, and the difference in the specified Q_{net} is shown in Figure 5a. These experiments enable us to conclude that the change of Q_{net} can have a moderate effect on the zonal surface temperature gradient. As Q_{net} decreases in the western equatorial Pacific, SSTs increase there and the zonal SST gradient exhibits an increase in the local region.

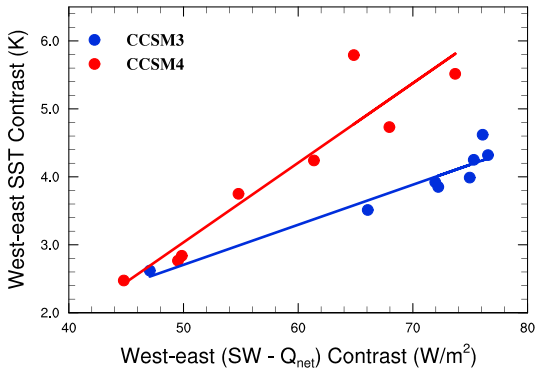

Figure 6. Relationship between west-east (SW-Q_{net}) contrast and west-east SST contrast. SW is all-sky surface net shortwave flux, and Q_{net} is net heat flux into the ocean (equation (1)). Blue dots are for CCSM3 and red dots for CCSM4. The lines are corresponding line regressions. The west-east contrast is defined by the difference between [5°S to 5°N, 150°E to 170°E] and [5°S to 5°N, 115°W to 95°W].

In summary, based on the analyses of the trends of surface energy fluxes, we find that the main processes associated with the changes of the zonal SST gradient as pCO_2 is increased are shortwave radiation (SW; mostly contributed by cloud response) and ocean adjustment. Figure 6 illustrates the relationship between SW-Q_{net} and the zonal SST contrast. In general, a larger SW-Q_{net} contrast between the western Pacific and the eastern Pacific

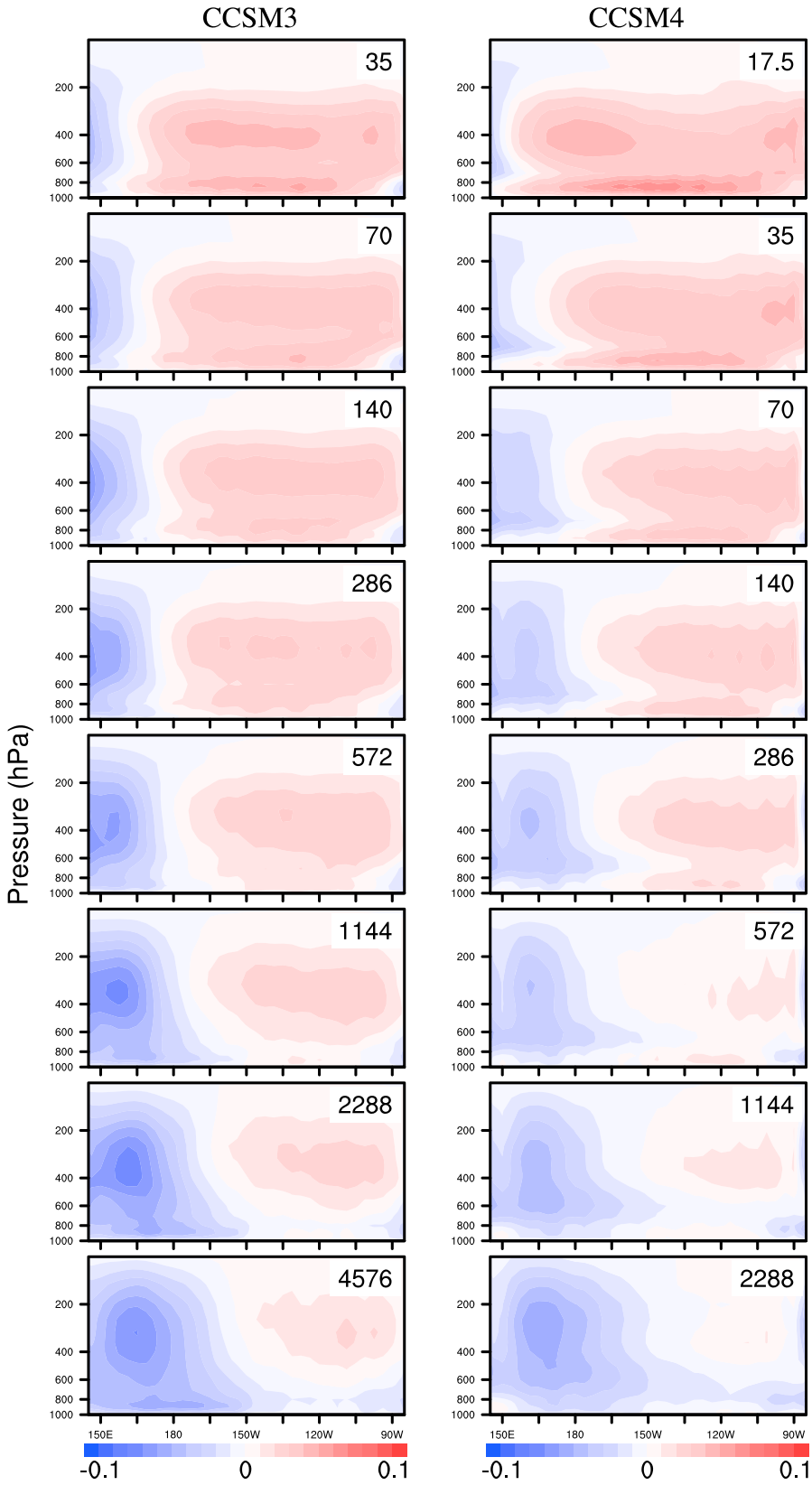

Figure 7. Atmospheric vertical velocity as a function of pressure and longitude at the deep tropics (meridional mean between 5°S and 5°N) of the Pacific Ocean, with negative values representing updrafts, for CO_2 concentrations of 35 to 4576 ppmv in (left column) CCSM3 and of 17.5 to 2288 ppmv in (right column) CCSM4. The unit is Pa s^{-1}.

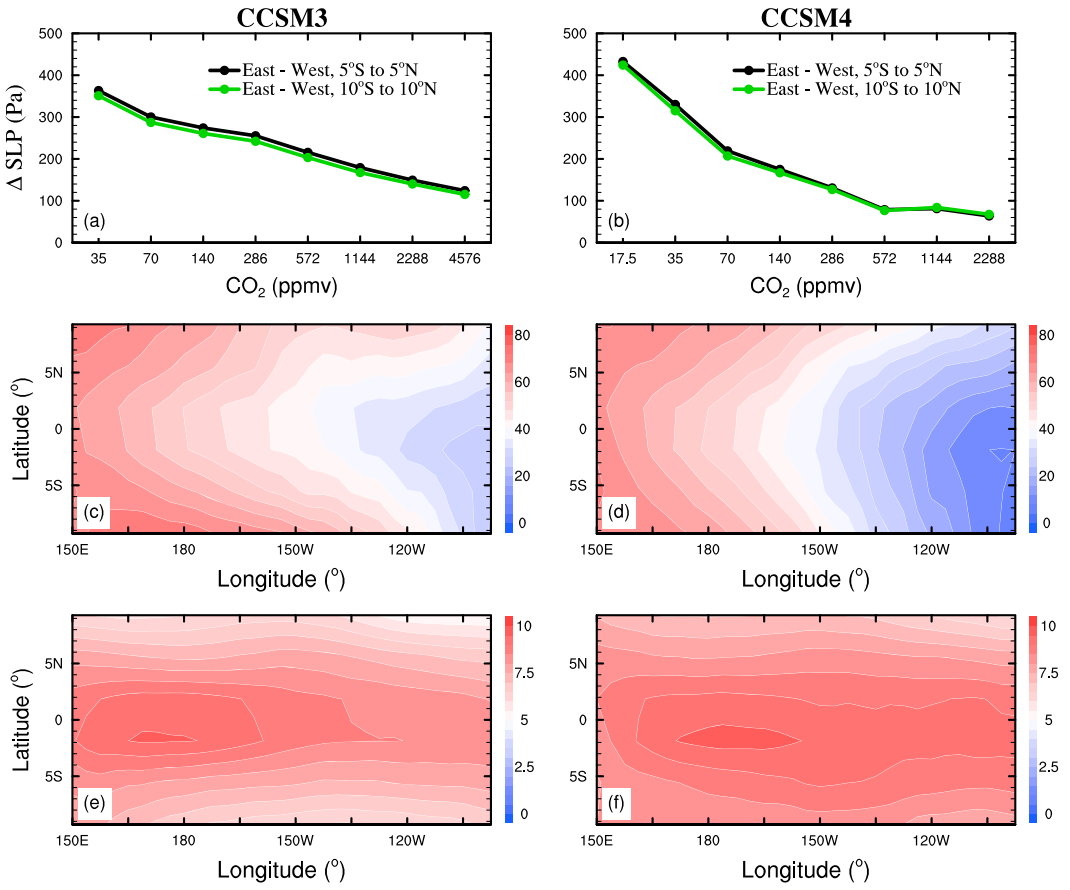

Figure 8. (a, b) Differences in sea level pressure (SLP, units: Pa) between the eastern Pacific (115°W–95°W, and 5°S–5°N or 10°S–10°N) and the western Pacific (150°E–170°E and 5°S–5°N or 10°S–10°N). (c, d) Linear trend of SLP of the Pacific for each doubling of CO_2 concentration. (e, f) Linear trend of atmospheric water (vapor, liquid, plus ice; unit: kg m^{-2}) content. Note that in climatology the eastern Pacific has higher SLPs than the western Pacific, and the equivalent pressure of 10 kg m^{-2} water is 100 Pa.

corresponds to a greater zonal SST gradient, in both CCSM3 and CCSM4. This relationship confirms our finding that the zonal SST gradient is mainly controlled by the combined effect of shortwave radiation and ocean adjustment. Moreover, from Figures 1e and 1f, it follows that the changes of the zonal SST gradient in the experiments of 70 to 1144 ppmv CO_2 of CCSM3 and in the experiments of 572 to 2288 ppmv CO_2 of CCSM4 are very small; this is due to the fact that the changes of west-east SW-Q_{net} contrast are small in these experiments (Figure 6), although the individual changes of west-east SW or Q_{net} contrast are much greater (figure not shown).

3.4. Changes in Atmospheric Circulation

The experiments covering a wide range of pCO_2 in CCSM3 and CCSM4 clearly show that the atmospheric circulation changes as pCO_2 is increased, including a weakening of atmospheric vertical subsidence in the central and eastern Pacific, an eastward expanse of the deep convection region (Figure 7), a decrease of zonal surface wind stresses (Figure 2), and a reduction of the zonal sea level pressure (SLP) gradient (Figure 8). As shown in Figure 7, the large-scale subsiding motion in the central and eastern Pacific weakens as climate warms, but the large-scale ascending motion in the western Pacific is enhanced and expands to the east. In our simulations, therefore, the response of atmospheric circulation cannot be simply summarized as a weakening of the Walker circulation, which was usually found in the experiments of doubling or quadrupling of pCO_2 in previous studies [e.g., *Dinezio et al.*, 2009].

For the surface wind stresses of the deep tropical Pacific, there are two significant trends, namely, increases in the meridional wind stresses and decreases in the zonal wind stresses especially along the equator (Figure 2). The increase of the meridional wind stresses may be associated with the enhanced equatorial warming

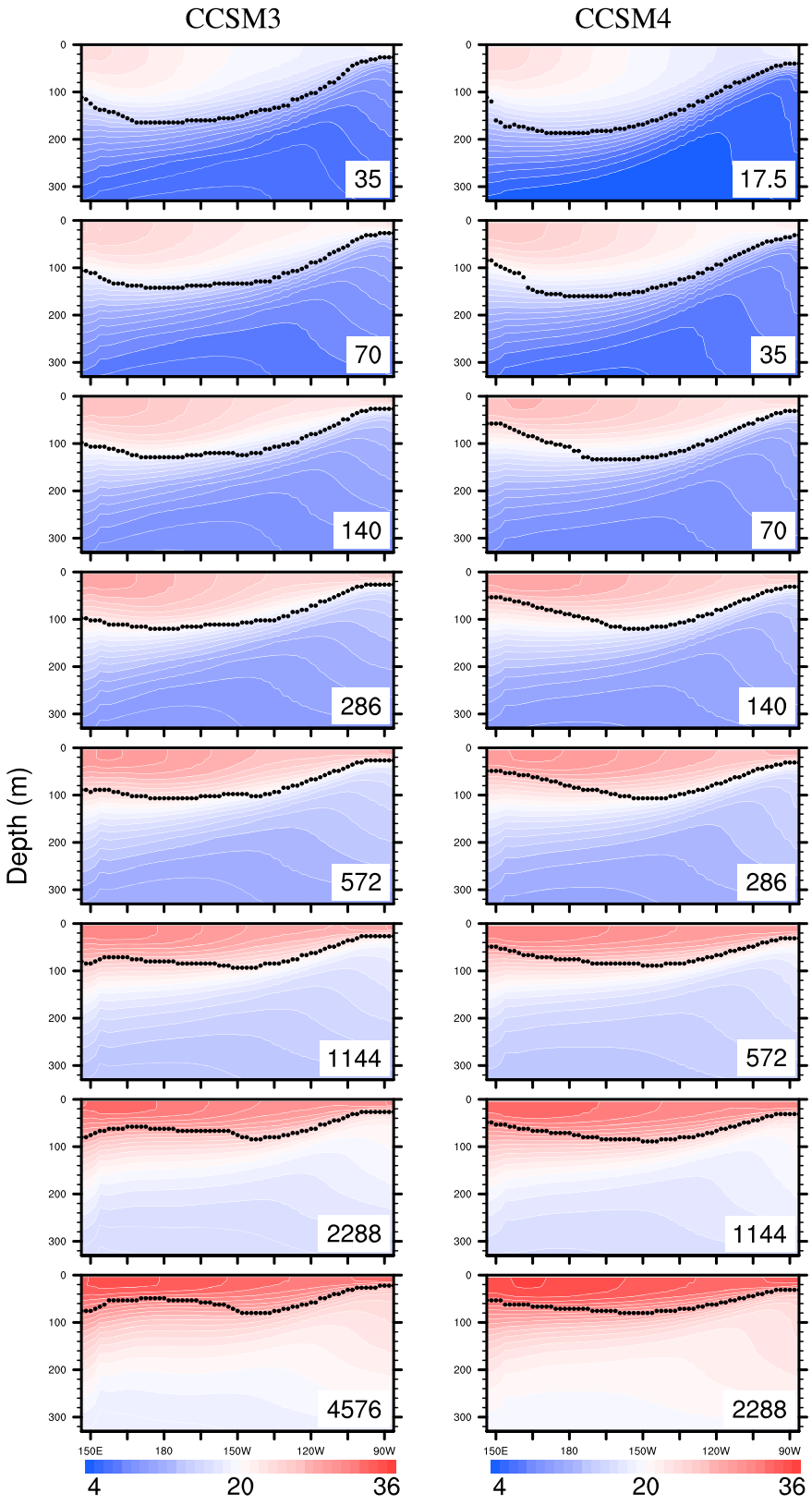

Figure 9. Ocean potential temperature (°C) as a function of depth and longitude at the deep tropics (meridional mean between 5°S and 5°N) of the upper Pacific Ocean, for CO_2 concentrations of 35 to 4576 ppmv in (left column) CCSM3 and of 17.5 to 2288 ppmv in (right column) CCSM4. The thermocline (black dots) is defined by a thin layer where the vertical gradient of ocean potential temperature is a local maximum [*Yang and Wang*, 2009].

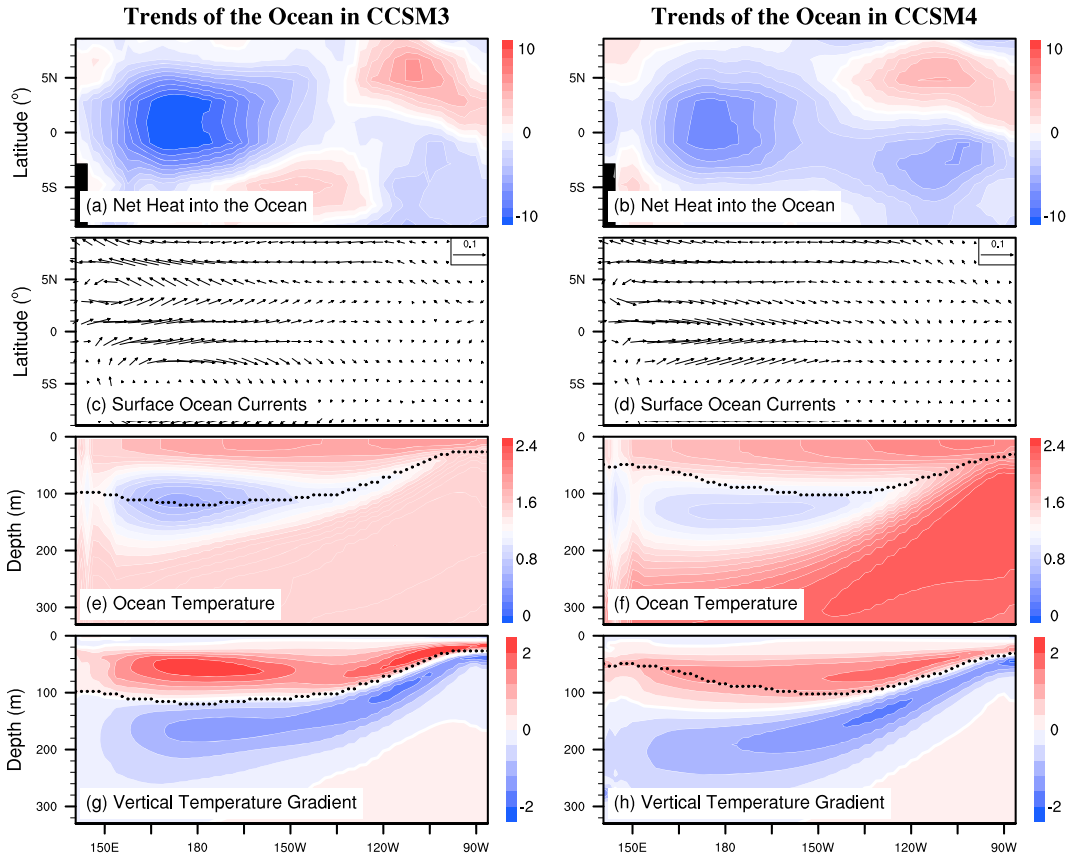

Figure 10. Linear trends of the tropical Pacific Ocean for each doubling of CO_2 concentration. (a, b) Net heat flux into the ocean, (c, d) surface ocean currents, (e, f) upper ocean temperature, and (g, h) vertical ocean temperature gradient. The units are, respectively, W m^{-2}, 0.1 m s^{-1}, K, and 0.01 K m^{-1} for each doubling of CO_2 concentration. The black dots in Figures 10e–10h are the thermocline of the control experiments for the preindustrial condition. Note that Figures 10a and 10b are the same as Figures 4m and 4n, but the resolution is for the ocean grid, which is higher than that for the atmosphere grid.

(EEW; Figure 2) and the strengthened Hadley cells (figure not shown). The EEW increases the meridional temperature gradient in the deep tropics and thereby promotes stronger meridional wind stresses. The decrease of the zonal wind stresses may be due to the combined effect of the decrease of the zonal SST gradient and the eastward shift of the Walker cell (Figure 7). The eastward shift of the Walker cell is accompanied by an anomaly of eastward surface wind stresses on the west side of the atmospheric ascending center.

As pCO_2 is increased, SLP increases in both eastern and western Pacific (Figures 8c and 8d). In a warmer climate, the increase of vertically integrated water content in the atmosphere acts to increase the SLP. In the deep tropics, the increase of water content is approximately 10 kg m^{-2}, corresponding to an equivalent increase of SLP by 100 Pa. The net increase of SLP, however, is less than this magnitude, thereby implying that atmospheric dynamical adjustment acts to decrease SLP especially in the eastern Pacific. More importantly, the increasing magnitude of SLP in the western Pacific is larger than that in the eastern Pacific (Figures 8c and 8d), so that the zonal SLP gradient (east minus west) decreases (Figures 8a and 8b). The decrease of the zonal SLP gradient is consistent with the weakening of the zonal surface wind stresses and with the slowing down of the atmospheric circulation although it occurs only in the central and eastern Pacific in our simulations.

3.5. Ocean Adjustment

As pCO_2 is increased, driven by the weakened zonal wind stresses, thermocline depth decreases (Figure 9), ocean upwelling in the eastern Pacific weakens (figure not shown), and the speed of surface ocean current decreases especially in the western and central Pacific (Figures 10c and 10d). For instance, in the experiments with 17.5, 286, and 2288 ppmv of CO_2 in CCSM4, the thermocline depth at 150°W longitude is approximately 160, 100, and 75 m, respectively (Figure 9). Furthermore, the magnitude of the shoaling in the eastern

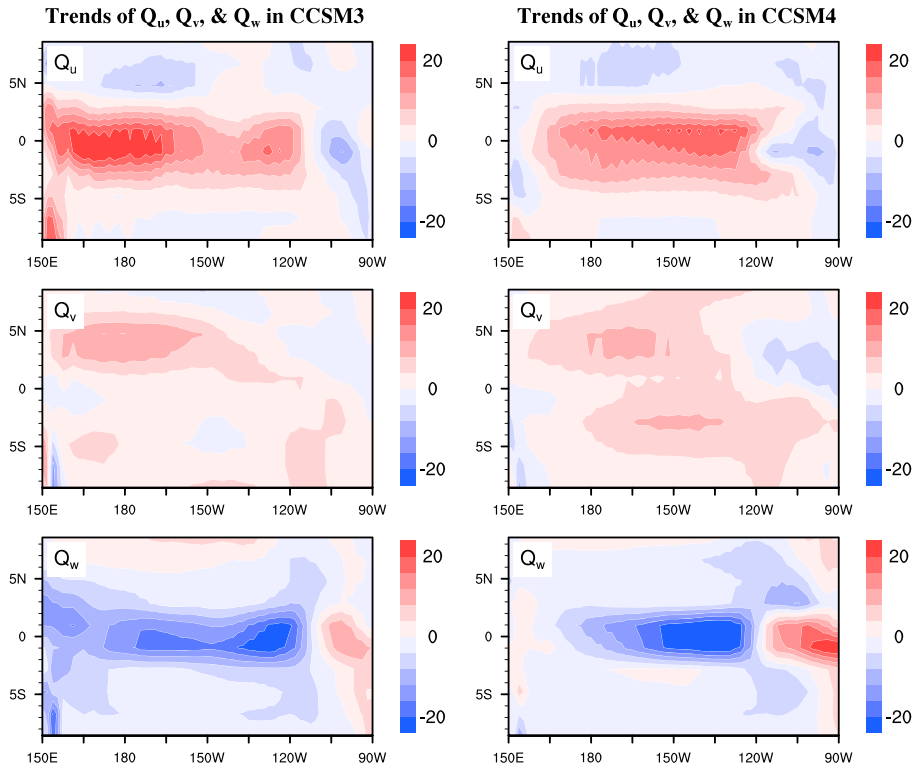

Figure 11. Trends of the divergences of (top row) zonal ocean heat transport (Q_u), (middle row) meridional ocean heat transport (Q_v), and (bottom row) vertical ocean heat transport (Q_w) vertically integrated from the sea surface to the depth of 75 m, in response to doubling atmospheric CO_2 concentration in CCSM3 (left column) and CCSM4 (right column). Positive values imply heating of the ocean surface layer. The contour interval is 2 W m^{-2}. The calculation follows the method of *Dinezio et al.* [2009].

Pacific is much smaller than that in the central and western Pacific, so that the west-east tilt of the thermocline decreases. Moreover, the responses of ocean dynamics are consistent with the decreasing trend of surface net heat flux into the equatorial Pacific Ocean shown in Figures 10a and 10b.

The changes of ocean vertical thermal structure are also not uniform, a minimum warming occurs around the thermocline at depths of about 80–180 m in the western Pacific; i.e., the warming at the sea surface and in the region below the thermocline is greater than that around the thermocline (Figures 10e and 10f). This phenomenon is very common among climate models as greenhouse gas forcing is increased; the simulations of *Vecchi and Soden* [2007], *Dinezio et al.* [2009], *Burls and Fedorov* [2014b], and *Luo et al.* [2015] with different climate models show the same phenomenon; and it could be a result of the shoaling of the thermocline, which brings deeper and colder waters upward [*Vecchi and Soden*, 2007; *Dinezio et al.*, 2009]. Moreover, the vertical temperature gradient (i.e., thermal stratification) increases in the wind-mixed upper ocean and decreases below the thermocline (Figures 10g and 10h). These trends of ocean vertical temperature gradients in our simulations are in qualitative agreement with that of the multimodel mean ocean response to doubling pCO_2 shown in *Dinezio et al.* [2009] and *Collins et al.* [2010]. Note that Figure 10f shows that the warming of the region below the thermocline in the western Pacific is slightly greater than that at the sea surface; this is due to the fact that the CCSM4 experiment with the highest CO_2 concentration of 2288 ppmv has not reached a final equilibrium during the integration.

The divergences of vertically integrated ocean heat transport between the sea surface and the depth of 75 m is shown in Figure 11 below. As CO_2 concentration is increased, the change of zonal heat transport divergence is positive in most of the equatorial Pacific, implying a heating effect on the upper ocean. The zonal heat transport divergence shows an enhanced equatorial band, which is due to the combined effect of weakened zonal currents and decreased zonal temperature gradients. The meridional heat transport divergence shows off-equatorial maxima in both hemispheres, which is because of the increased meridional temperature gradients associated with enhanced equatorial warming. Both responses of the zonal and meridional heat

transport divergences represent dynamical heating effects in the equatorial Pacific. The vertical heat transport divergence shows a decreasing trend across the equatorial Pacific except in the vicinity of 90°W. This is due to the increase of ocean thermal stratification, although the ocean upwelling becomes weaker [*Dinezio et al.*, 2009]. In the region around 90°W, the change of vertical heat transport divergence is positive, because of that the weakened ocean upwelling exceeds the enhanced thermal stratification. Note that in these calculations, the effects of subgrid mixing and submonth variability are not considered, since they are unavailable from model default output.

4. Discussions

This study is relevant to ongoing research concerning expectations of the variations of the zonal SST gradient under both future and a variety of past climate conditions. The monotonic behavior of the zonal SST gradient makes it be relatively easy to predict its trend as pCO_2 is changed. For the ongoing climate change due to increases of anthropogenic greenhouse gases, our simulations suggest that a decreasing trend in the zonal SST gradient is to be expected with high confidence, but the magnitude of the change is model dependent. If pCO_2 is decreased from 286 to 140 ppmv that is somewhat lower than the value during the Last Glacial Maximum (LGM) at ≈21,000 years ago, our simulations imply an increase in the zonal SST gradient by 0.5°C in CCSM3 and by 1.0°C in CCSM4. Our simulations, however, have not included the expanded continental ice sheets that formed during the LGM [*Peltier and Solheim*, 2004], which are expected to have had a further influence on the zonal SST gradient.

In the case of 4576 ppmv of CO_2 in CCSM3, the climate system enters a state with a very weak zonal SST gradient; in CCSM4, it requires a relatively lower pCO_2 to obtain a similar state; but, pCO_2 in the early Pliocene was only 330−380 ppmv [*Fedorov et al.*, 2013]. Our results suggest that the increased pCO_2 (compared to the preindustrial level), would have contributed to the weak zonal SST gradient during the early Pliocene, but its magnitude is much smaller than that which the geochemical proxy data have suggested. Other missing physical processes might also have contributed to the very weak zonal SST gradient during that epoch, and further exploration will be required to identify them.

Based on the large coverage of pCO_2 examined in our simulations, we find some new results that are quite different from those of conventional investigations based on only doubling or quadrupling pCO_2. In our simulations, the increasing rate of global-mean atmospheric water (vapor, liquid, and ice) content is about 7% per 1 K increasing in global-mean surface temperature (Figure 12a), and the increasing rate of global-mean precipitation is about 2% per 1 K of surface warming (Figure 12b). These results are consistent with those found in other models [*Held and Soden*, 2006; *Collins et al.*, 2010]. When the same calculations are performed but only for the tropics, very similar trends in area-mean atmospheric water content and precipitation are found (Figures 12c and 12d). This would suggest a weakening of the Walker circulation if following the proposal of *Vecchi et al.* [2006]; however, we find that the weakening occurs only in the central and eastern Pacific, whereas in the western Pacific the atmospheric circulation becomes stronger (see Figure 7). Further analyses will be required to explain the differences.

We do not find superrotation developing at high CO_2 concentrations in our simulations (figure not shown). However, this cannot be taken as a proof that the hypothesis of *Tziperman and Farrell* [2009] is incorrect. The key aspect of their hypothesis is the response of convection and clouds to the warming associated with increasing greenhouse gas concentrations. Present general circulation models are not able to well simulate convection and clouds, so that our results cannot exclude their hypothesis. Future works with a superparameterized climate model (such as *Arnold et al.* [2014]) or a near-global (or global) cloud-resolving model (such as *Bretherton and Khairoutdinov* [2015]) will be required to further investigate this.

Besides the change of the zonal SST gradient, the meridional SST gradient also changes. In both CCSM3 and CCSM4, the warming in the deep tropics is greater than that in the subtropics (see Figure 2), i.e., an enhanced equatorial warming, which may be mainly associated with wind-evaporation-SST feedback [*Liu et al.*, 2005; *Xie et al.*, 2010]. Moreover, the warming of the polar regions is greater than that of the tropics, so that the equator-to-pole surface temperature difference decreases, i.e., a tendency of polar amplification.

It would be helpful if we could separate the cause and effect between clouds and SSTs, between surface heat fluxes and ocean heat transport, and between near-surface wind stresses and SSTs. However, this task is always very difficult or even impossible in a fully coupled, nonlinear atmosphere-ocean system. This is because of

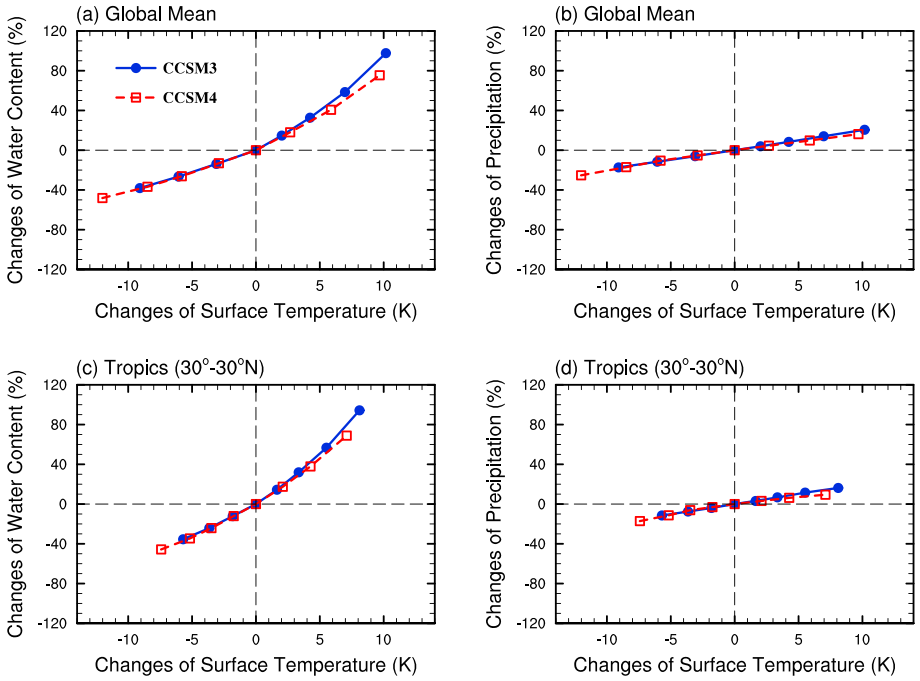

Figure 12. Changes of atmospheric water (vapor, liquid, and ice) content, precipitation, and surface temperature in all the simulations, respective to the control runs of the preindustrial condition. The blue line is CCSM3 and red CCSM4. (a–b) For global mean and (c–d) for the tropical mean between 30°S and 30°N.

the fact that all of the processes work together to determine the final equilibrium state of the system, and there are many tight feedback processes connecting them. For instance, in coupled models, the change of ocean heat transport is the result of the balance between radiation, surface evaporation, ocean dynamics, and sensible heat exchanges between atmosphere and ocean; changes of vertical and horizontal ocean advection can influence ocean heat transport, but it is not in a uniquely identifiable manner; changes of cloud radiative forcing can also affect the surface radiation fluxes and thereby the energy of ocean heat transport. Recently, a "cloud locking method" [e.g., *Voigt and Shaw*, 2015] and a "surface wind locking method" [e.g., *Koll and Abbot*, 2013; *Luo et al.*, 2015] have been employed to separate the different processes of the climate system. However, these methods have been used in atmosphere-only or ocean-only circulation models, and further work will be required to employ them in fully coupled atmosphere-ocean model(s).

Finally, we should note that in model simulations of the effects of increasing anthropogenic greenhouse gases, there are large uncertainties in projecting the trends of clouds [e.g., *Bony and Dufresne*, 2005] and of the tropical atmospheric circulation [e.g., *Kociuba and Power*, 2015], which are the key mechanisms in determining the zonal SST gradient. Our results are not expected to be reproducible in all other climate models. Nevertheless, we note that *Cherchi et al.* [2008] employed the fully coupled atmosphere-ocean model, SINTEXG, to simulate the climates of pCO_2 from 353 to 5648 ppmv. They also obtained a decreasing trend of the zonal SST gradient with increasing pCO_2. Our work provides a further benchmark for future studies of the zonal SST gradient of the equatorial Pacific.

5. Conclusion

The two fully coupled climate models, CCSM3 and CCSM4, have been employed to investigate the response of the mean equatorial climate state to a wide range of atmospheric pCO_2. We find the zonal SST gradient along the equatorial Pacific to be an almost monotonically decreasing function of pCO_2 in the two models. As illustrated schematically in Figure 13, under cold climate conditions with a very low pCO_2, the zonal trade winds become very intense, and these winds drive a strong ocean upwelling, which acts to cool the equatorial Pacific. Under hot climate conditions with a very high pCO_2, the zonal trade winds become very weak, which serves to decouple the connection between the cool thermocline water and the warm surface water. The present-day climate is between the end-member cold and hot states. As pCO_2 is gradually increased from a

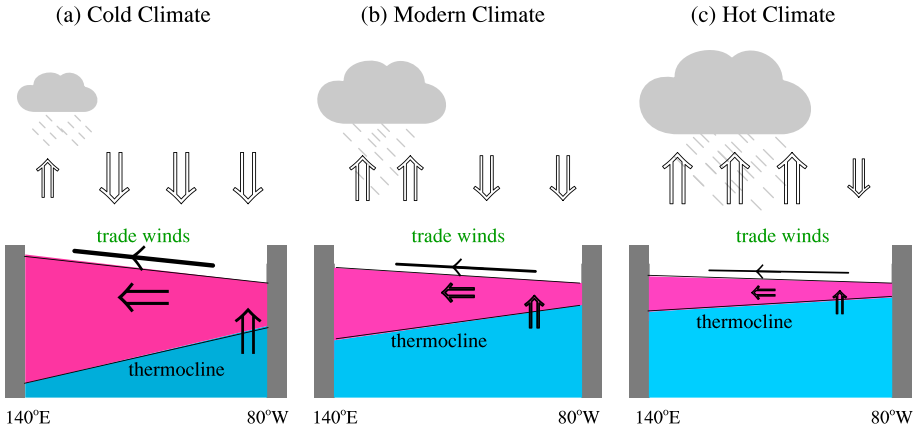

Figure 13. Schematic diagram of the time-mean characteristics of the equatorial Pacific in (a) cold, (b) modern, and (c) hot climate states under different CO_2 concentrations. See text for detailed descriptions.

very low level to a very high level, both atmosphere and ocean become warmer; the thermocline becomes shallower and flatter; sea level pressure difference between the eastern and western Pacific decreases; the zonal SST gradient becomes weaker; motions of the atmosphere and ocean slow down, including the ocean upwelling in the cold tongue region, surface ocean currents, zonal equatorial trade winds, and atmospheric subsiding motion over the eastern Pacific; over the western Pacific, atmospheric ascending motion enhances and expands eastward; meanwhile, the optical depth of clouds increase in this region and convective clouds expand eastward. The optical depth of clouds over the western and central Pacific is much larger in the hot climate state than in the cold climate state, which strongly cools the surface.

Acknowledgments

We thank two anonymous reviewers for their extremely helpful comments and suggestions that have enabled us to significantly improve the article. We are grateful to Gan Zhang and Shineng Hu for their insightful comments on the manuscript, and to Guido Vettoretti for technical assistance. Y.H. and J.Y. are supported by the National Natural Science Foundation of China (NSFC) under grants 41375072 and 41025018. J.Y. was partially supported by the Over-sea Study Program for Graduate Students of the China Scholarship Council, for the 2 years spent visiting the University of Toronto. The research of W.R.P. at Toronto is supported by the NSERC Discovery grant A9627. The required computations were performed on the SciNet facility at the University of Toronto, which is a component of the Compute Canada HPC platform. If data from the climate simulations are required, it is available through email, J.Y.: junyang@pku.edu.cn.

References

Alexander, M. A., I. Blade, M. Newman, J. R. Lanzante, N.-C. Lau, and J. D. Scott (2002), The atmospheric bridge the influence of ENSO teleconnections on air-sea interaction over the global oceans, *J. Clim.*, *15*, 2205–2231.

Arnold, N. P., M. Branson, M. A. Burt, D. S. Abbot, Z. Kuang, D. A. Randall, and E. Tzipermann (2014), Effects of explicit atmospheric convection at high CO_2, *Proc. Natl. Acad. Sci. U.S.A.*, *111*(30), 10943–10948.

An, S.-I., J.-W. Kim, S.-H. Im, B.-M. Kim, and J.-H. Park (2012), Recent and future sea surface temperature trends in tropical Pacific warm pool and cold tongue regions, *Clim. Dyn.*, *29*, 1373–1383.

Barreiro, M., and S. G. Philander (2008), Response of the tropical Pacific to changes in extratropical clouds, *Clim. Dyn.*, *31*, 713–729.

Bjerknes, J. (1969), Atmospheric teleconnections from the equatorial Pacific, *Mon. Weather Rev.*, *97*, 163–172.

Bony, S., and J.-L. Dufresne (2005), Marine boundary layer clouds at the heart of tropical cloud feedback uncertainties in climate models, *Geophy. Res. Lett.*, *32*, L20806, doi:10.1029/2005GL023851.

Boucher, O., J. Haigh, D. Hauglustainse, J. Haywood, G. Myhre, T. Nakajima, G. Y. Shi, and S. Solomon (2001), Chapter 6.3.1. Carbon Dioxide, in *Climate Change 2001: The Scientific Basis*, Cambridge Univ. Press, U. K.

Bretherton, C., and M. F. Khairoutdinov (2015), Convective self-aggregation feedbacks in near-global cloud resolving simulations of an aquaplanet, *J. Adv. Modell. Earth Syst.*, *32*(7), 1765–1787.

Burls, N. J., and A. V. Fedorov (2014a), What controls the mean east-west sea surface temperature gradient in the equatorial Pacific: The role of cloud albedo, *J. Clim.*, *27*, 2757–2779.

Burls, N. J., and A. V. Fedorov (2014b), Simulating Pliocene warmth and a permanent El Niño-like state: The role of cloud albedo, *Paleoceanography*, *29*, 893–910, doi:10.1002/2014PA002644.

Chiang, J. C. H. (2009), The tropics in paleoclimate, *Annu. Rev. Earth Planet. Sci.*, *37*, 263–297.

Cherchi, A., S. Masina, and A. Navarra (2008), Impact of extreme CO_2 levels on tropical climate: A CGCM study, *Clim. Dyn.*, *31*, 743–758.

Clement, A. C., R. Seager, M. A. Cane, and S. E. Zebiak (1996), An ocean dynamical thermostat, *J. Clim.*, *9*, 2190–2196.

Collins, M., and CMIP Modeling Groups (2005), El Niño- or La Niña-like climate change?, *Clim. Dyn.*, *24*(1), 89–104.

Collins, W. D., et al. (2006a), The community climate system model version 3 (CCSM3), *J. Clim.*, *19*, 2122–2143.

Collins, W. D., et al. (2006b), Radiative forcing by well-mixed greenhouse gases: Estimates from climate models in the Intergovernmental Panel on Climate Change (IPCC) Fourth Assessment Report (AR4), *J. Geophys. Res.*, *111*, D14317, doi:10.1029/2005JD006713.

Collins, M., et al. (2010), The impact of global warming on the tropical Pacific Ocean and El Niño, *Nat. Geosci.*, *3*, 391–397.

Deser, C., A. S. Phillips, and M. A. Alexander (2012), Twentieth century tropical sea surface temperature trends revisited, *Geophy. Res. Lett.*, *37*(10), L10701, doi:10.1029/2010GL043321.

Deser, C., et al. (2012), ENSO and Pacific decadal variability in the community climate system model version 4, *J. Clim.*, *25*, 2622–2651.

Dinezio, P. N., A. C. Clement, G. A. Vecchi, B. J. Soden, B. P. Kirtman, and S. K. Lee (2009), Climate response of the equatorial Pacific to global warming, *J. Clim.*, *22*, 4873–4892.

Emanuel, K. (2001), Contribution of tropical cyclones to meridional heat transport by the oceans, *J. Geophy. Res.*, *106*(D14), 14771–14781.

Fang, C., and L. Wu (2008), The role of ocean dynamics in tropical Pacific SST response to warm climate in a fully coupled GCM, *Geophy. Res. Lett.*, *35*, L08703, doi:10.1029/2007GL033097.

Fedorov, A. V., P. S. Dekens, M. McCarthy, A. C. Ravelo, P. B. deMenocal, M. Barreiro, R. C. Pacanowski, and S. G. Philander (2006), The Pliocene paradox (mechanisms for a permanent El Niño), *Science*, *312*, 1485–1489.

Fedorov, A. V., C. Brierley, and K. Emanuel (2010), Tropical cyclones and permanent El Niño in the early Pliocene, *Nature*, *463*, 1066–1070.

Fedorov, A. V., C. Brierley, L. Lawrence, Z. Liu, P. Dekens, and A. C. Ravelo (2013), Patterns and mechanisms of early Pliocene warmth, *Nature*, *496*, 43–49.
Gent, P. R., et al. (2011), The community climate system model version 4, *J. Clim.*, *24*, 4973–4991.
Hartmann, D. L., and M. L. Michelsen (1993), Large-scale effects on regulation of tropical sea surface temperature, *J. Clim.*, *6*, 2049–2062.
Held, I. M., and B. J. Soden (2006), Robust responses of the hydrological cycle to global warming (2006), *J. Clim.*, *19*, 5686–5699.
Haywood, A. M., et al. (2013), Large-scale features of Pliocene climate: Results from the Pliocene Model Intercomparison Project, *Clim. Past*, *9*, 191–209.
Haywood, A. M., H. J. Dowsett, A. M. Dolan, D. Rowley, B. Otto-Bliesner, M. A. Chandler, S. J. Hunter, D. J. Lunt, M. Pound, and U. Salzmann (2016), The Pliocene Model Intercomparison Project (PlioMIP) Phase 2: Scientific objectives and experimental design, *Clim. Past*, *12*, 663–675.
Jansen, M., and R. Ferrari (2009), Impact of the latitudinal distribution of tropical cyclones on ocean heat transport, *Geophys. Res. Lett.*, *36*, L06604, doi:10.1029/2008GL036796.
Kociuba, G., and S. B. Power (2015), Inability of CMIP5 models to simulate recent strengthening of the walker circulation: Implications for projections, *J. Clim.*, *28*, 28–35.
Koll, D., and D. S. Abbot (2013), Why tropical sea surface temperature is insensitive to ocean heat transport changes, *J. Clim.*, *26*, 6742–6749, doi:10.1175/JCLI-D-13-00192.1.
Knutson, T. R., and S. Manabe (1995), Time-mean response over the tropical Pacific to increased CO_2 in a coupled ocean atmosphere model, *J. Clim.*, *8*, 2181–2199.
Li, G., S.-P. Xie, Y. Du, and Y. Luo (2016), Effects of excessive equatorial cold tongue bias on the projections of tropical Pacific climate change. Part I: The warming pattern in CMIP5 multi-model ensemble, *Clim. Dyn.*, *1–15*, doi:10.1007/s00382-016-3043-5.
Liu, Z., and B. Huang (1997), A coupled theory of tropical climatology: Warm pool, cold tongue, and Walker circulation, *J. Clim.*, *10*, 1662–1679.
Liu, Z., S. Vavrus, F. He, N. Wen, and Y. Zhong (2005), Rethinking tropical ocean response to global warming: The enhanced equatorial warming, *J. Clim.*, *18*, 4684–4700.
Li, X., S.-P. Xie, S. T. Gille, and C. Yoo (2015), Atlantic-induced pan-tropical climate change over the past three decades, *Nat. Clim. Change*, *6*, 275–280.
Luo, Y., J. Lu, F. Liu, and W. Liu (2015), Understanding the El Niño-like oceanic response in the tropical Pacific to global warming, *Clim. Dyn.*, *45*, 1945–1964.
Meehl, G. A., and Washington W. M. (1996), El Niño-like climate change in a model with increased atmospheric CO_2 concentrations, *Nature*, *382*, 56–60.
Meehl, G. A., et al. (2007), Global climate projections, in *Climate Change 2007: The Physical Science Basis*, edited by S. Solomon et al., pp. 747–845, Cambridge Univ. Press, U. K., and New York.
Merlis, T. M., and T. Schneider (2011), Changes in zonal surface temperature gradients and Walker circulations in a wide range of climates, *J. Clim.*, *24*, 4757–4768.
Molnar, P., and M. A. Cane (2007), Early Pliocene (pre-ice age) El Niño–like global climate: Which El Niño?, *Geosphere*, *3*(5), 337–365.
Peltier, W. R., and L. P. Solheim (2004), The climate of the Earth at Last Glacial Maximum: Statistical equilibrium state and a mode of internal variability, *Quat. Sci. Rev.*, *23*, 335–357.
Pierrehumbert, R. T. (1995), Thermostats, radiator fins, and the runaway greenhouse, *J. Atmos. Sci.*, *52*, 1784–1806.
Scroxton, N., S. G. Bonham, R. E. M. Rickaby, S. H. F. Lawrence, M. Hermoso, and A. M. Haywood (2011), Persistent El Niño–Southern Oscillation variation during the Pliocene Epoch, *Paleoceanography*, *26*, PA2215, doi:10.1029/2010PA002097.
Song, X., and G. J. Zhang (2014), Role of climate feedback in El Niño-like SST response to global warming, *J. Clim.*, *27*, 7301–7318.
Tung, K.-K., and J. Zhou (2010), The Pacific's response to surface heating in 130 Yr of SST: La Niña-like or El Niño-like?, *J. Atmos. Sci.*, *67*, 2649–2657.
Tziperman, E., and B. Farrell (2009), Pliocene equatorial temperature: Lessons from atmospheric superrotation, *Paleoceanography*, *24*, PA1101, doi:10.1029/2008PA001652.
Vecchi, G. A., B. J. Soden, A. T. Wittenberg, I. M. Held, A. Leetma, and M. J. Harrison (2006), Weakening of tropical Pacific atmospheric circulation due to anthropogenic forcing, *Nature*, *441*, 73–76.
Vecchi, G. A., and B. J. Soden (2007), Global warming and the weakening of the tropical circulation, *J. Clim.*, *20*, 4316–4340.
Vecchi, G. A., A. Clement, and B. J. Soden (2008), Examining the tropical Pacifics response to global warming, *Eos, Trans. AGU*, *89*, doi:10.1029/2008EO090002.
Voigt, A., and T. Shaw (2015), Circulation response to warming shaped by radiative changes of clouds and water vapor, *Nat. Geosci.*, *8*, 102–106, doi:10.1038/ngeo2345.
Wallace, J. M. (1992), Effect of deep convection on the regulation of tropical sea surface temperature, *Nature*, *357*, 230–231.
Wara, M. W., A. C. Ravelo, and M. L. Delaney (2005), Permanent El Niño-like conditions during the Pliocene warm period, *Science*, *309*, 758–761.
Watanabe, T., et al. (2011), Permanent El Niño during the Pliocene warm period not supported by coral evidence, *Nature*, *471*, 209–211.
Wyrtki, K. (1975), El Niño—The dynamic response of the equatorial Pacific Ocean to atmospheric forcing, *J. Phys. Oceanogr.*, *5*, 572–584.
Xie, S.-P., C. Deser, G. A. Vecchi, J. Ma, H. Teng, and A. T. Wittenberg (2010), Global warming pattern formation: sea surface temperature and rainfall, *J. Clim.*, *23*, 966–986.
Yang, H., and F. Wang (2009), Revisiting the thermocline depth in the equatorial Pacific, *J. Clim.*, *22*, 3856–3863.
Yang, J., W. R. Peltier, and Y. Hu (2012a), The initiation of modern "soft Snowball" and "hard Snowball" climates in CCSM3. Part I: The influence of solar luminosity, CO_2 concentration and the sea-ice/snow albedo parameterization, *J. Clim.*, *25*, 2721–2736.
Yang, J., W. R. Peltier, and Y. Hu (2012b), The initiation of modern soft and hard Snowball Earth climates in CCSM4, *Clim. Past*, *8*, 907–918.
Yeh, S.-W., Y.-G. Ham, and J.-Y. Lee (2012), Changes in the tropical Pacific SST trend from CMIP3 to CMIP5 and its implication of ENSO, *J. Clim.*, *25*, 7764–7771.
Zhang, Y. G., M. Pagani, and Z. Liu (2014), A 12-million-year temperature history of the tropical Pacific Ocean, *Science*, *343*, 84–86.